Solid Freeform Fabrication 2017: Proceedings of the 28th Annual International Solid Freeform Fabrication Symposium – An Additive Manufacturing Conference
Reviewed Paper

MULTI-MATERIAL STRUCTURAL TOPOLOGY OPTIMIZATION UNDER UNCERTAINTY VIA A STOCHASTIC REDUCED ORDER MODEL APPROACH

M.A. Aguiló[1] and J.E. Warner[2]

[1]Sandia National Laboratories, 1515 Eubank SE, Albuquerque, NM 87123
[2]NASA Langley Research Center, 1 Nasa Dr, Hampton, VA 23666

Abstract

This work presents a stochastic reduced order modeling approach for the solution of uncertainty aware, multi-material, structural topology optimization problems. Uncertainty aware structural topology optimization problems are computationally complex due to the number of model evaluations that are needed to quantify and propagate design uncertainties. This computational complexity is magnified if high-fidelity simulations are used during optimization. A stochastic reduced order model (SROM) approach is applied to 1) alleviate the prohibitive computational cost associated with large-scale, uncertainty aware, structural topology optimization problems; and 2) quantify and propagate inherent uncertainties due to design imperfections. The SROM framework transforms the uncertainty aware, multi-material, structural topology optimization problem into a deterministic optimization problem that relies only on independent calls to a deterministic analysis engine. This approach enables the use of existing optimization and analysis tools for the solution of uncertainty aware, multi-material, structural topology optimization problems.

Introduction

A multi-material structural topology optimization problem in the case where the applied load and compliant material are considered to be random is solved to demonstrate the SROM approach. The randomness in the applied load and compliant material will be introduced through uncertainty in the orientation of the applied load and the elastic modulus of the compliant material. The optimal material distribution will be computed by solving the following uncertainty aware, multi-material, structural topology optimization problem

$$\begin{aligned} \mathscr{X}^* = \arg\min_{\mathscr{X}} :\ & C(\widehat{\mathscr{X}}) = E\left[\boldsymbol{U}^T[\boldsymbol{K}(\widehat{\mathscr{X}},\Sigma)]\boldsymbol{U}\right] = \sum_{m=1}^{M}\sum_{e=1}^{N_e}(z_m^e(\hat{\boldsymbol{x}}_m^k))^{\mu}E\left[\bar{\boldsymbol{u}}_e^T[\bar{\boldsymbol{k}}_e(\Sigma)]\bar{\boldsymbol{u}}_e\right] \\ \text{subject to} :\ & \boldsymbol{R}(\boldsymbol{U},\widehat{\mathscr{X}},\Sigma;\Theta) = \boldsymbol{0} \quad \text{in} \quad \Omega \quad \text{a.s.} \\ & : \sum_{m=1}^{M}\sum_{e=1}^{N_e} z_m^e(\hat{\boldsymbol{x}}_m^k)\gamma_m V_e \leq \mathrm{M}_{\max} \\ & : \boldsymbol{0} \leq \boldsymbol{x}_m \leq \boldsymbol{1}, \end{aligned} \tag{1}$$

where $\mathscr{X}^* = \{\boldsymbol{x}_m^*\}_{m=1}^M$ is the optimal set of control points, $\mathscr{X} = \{\boldsymbol{x}_m\}_{m=1}^M$ is the set of trial control points, and $\widehat{\mathscr{X}} = \{\hat{\boldsymbol{x}}_m\}_{m=1}^M$ is the set of filtered control points. Therefore, the total number of design variables $N_{\boldsymbol{x}} = M \times n_{\boldsymbol{x}}$, where M is the number of candidate materials and $n_{\boldsymbol{x}}$ is the number of control points. The number of control points is set to either the number of nodes or the number of

elements on the computational mesh. Therefore, the number of control points, $n_{\boldsymbol{x}}$, is the same for all candidate materials, hence $N_{\boldsymbol{x}} = M \times n_{\boldsymbol{x}}$. The density at the control points for a given candidate material is denoted by $\boldsymbol{x}_m$. The filtered densities associated with the k set of control points in finite element e and candidate material m is denoted by $\hat{\boldsymbol{x}}_m^k$. The filtered volume fraction in element e for candidate material m is denoted by z_m^e. The penalty constant that aims to push the volume fraction in element e to zero is denoted by $\mu > 1$ and N_e is the total number of finite elements.

In Equation (1), C is the expected value in the structural compliance, V_e is the volume of finite element e, $\mathrm{M}_{\max}$ is the mass or monetary limit, and γ_m is the mass density or cost of material m. The stiffness matrix assembled from random element stiffness matrices, $[\bar{\boldsymbol{k}}_e]$, is denoted by $[\boldsymbol{K}]$, The random global displacement vector is $\boldsymbol{U}$ and $\bar{\boldsymbol{u}}_e$ are the random displacements for element e. The random residual equation is denoted by $\boldsymbol{R}$ and the computational domain is denoted by $\Omega \subseteq \mathbb{R}^d,\ d \in \{1,2,3\}$. Finally, Σ is the random elastic modulus for the compliant material and Θ is the random orientation of an applied load.

The volume constraint is defined using the filtered volume fractions z_m^e for candidate material m, but the filtered densities at the control points, $\hat{\boldsymbol{x}}_m$, for candidate material m can be defined as nodal or element control points. Thus, given $\hat{\boldsymbol{x}}_m$, the filtered material density at each element for candidate material m is defined as:

$$z_m^e(\hat{\boldsymbol{x}}_m^k) = \frac{1}{\hat{n}_m^e} \sum_{k \in \mathscr{K}_m^e} \hat{\boldsymbol{x}}_m^k, \tag{2}$$

where $\hat{n}_m^e$ is the number of control points in the set $\mathscr{K}_m^e$ of control points associated with element e and candidate material m. If nodal control points are used in (2), $\hat{n}_m^e$ is equal to the number of nodes on finite element e. Contrary, if element control points are used, $\hat{n}_m^e = 1$.

Notice that in (1) the stochastic, multi-material, structural topology optimization problem is constrained by a system of stochastic algebraic equations

$$\boldsymbol{R}(\boldsymbol{U}, \widehat{\mathscr{X}}, \Sigma; \Theta) = [\boldsymbol{K}(\widehat{\mathscr{X}}, \Sigma)]\boldsymbol{U} - \boldsymbol{F}(\Theta), \tag{3}$$

where $\boldsymbol{F}$ is the random global force vector. The global displacement and force vectors are now random in (3) through their dependence on the random orientation of the applied load and the elastic modulus of the compliant material. The solution of (1) depends on the suitable parameterization of Σ and Θ to make the solution of the stochastic partial differential equation and the evaluation of the expected value in the structural compliance tractable. This paper will focus on the application of SROMs as an efficient means of quantifying and propagating the uncertainty in Σ and Θ for the solution of (1).

The remainder of this article is organized as follows. In the next section, the motivation for this work is discussed. In the following section, 1) the deterministic, multi-material, structural topology optimization formulation, 2) the generic description of the SROM approach, and 3) the uncertainty aware, multi-material, structural topology optimization formulation based on an SROM representation of the random parameters are presented. In this section, the gradient derivation for the uncertainty aware, multi-material, structural topology optimization problem using stochastic

reduced order models (SROMs) and the core steps for computing the objective function and gradient are also presented. Next, a two-dimensional, multi-material, structural topology optimization example that highlights the advantages of SROMs for uncertainty quantification and propagation is presented. Finally, the article concludes with a summary of this work.

Motivation

The intersection of additive processes and design optimization has introduced revolutionary capabilities for design, product development, and manufacturing. "Complexity is free" has been a common mantra with additive manufacturing processes [1]. However, anyone involved in the qualification or certification of additive processes or materials will acknowledge that complexity is currently not free due to the prevailing lack of understanding of advanced manufacturing processes [1]. One approach to address the stochastic nature of additive processes is to improve process determinism. An alternate, complementary approach is to account for these inherent uncertainties early in the design process by providing designers with uncertainty aware computational design tools that generate solutions that insure performance requirements are met and margins are quantified.

Uncertainties abound in any design scenario and include sources from requirements, boundary conditions, and environments; not just process capabilities, feedstocks, and final material properties. Advanced uncertainty quantification and propagation methodologies have been available for years [2, 3, 4], but even the most basic capabilities for design under uncertainty [5, 6, 7] remain unavailable to end users. Since existing tools do not account for uncertainties during analyses, there is no guarantee that their solutions are robust to these sources of uncertainty. While holding great potential and value for product performance and qualification, design under uncertainty is a significant challenge due to the computational resources necessary to create high-fidelity solutions. This computational toll limits the design iterations available to explore solutions robust to uncertainties. Therefore, to make design under uncertainty an integral part of the design process, critical algorithmic issues must be solved. First, novel sampling algorithms are needed to reduce sample sizes required to accurately quantify and propagate multiple sources of uncertainty. Second, algorithms must efficiently utilize all available computing resources to increase performance, speed, and accuracy. Third, these novel algorithms should be integrated into a reliable computational design tool accessible to end users.

A relatively untapped benefit of additive manufacturing is its potential to control material at the voxel level. This feature expands the design space available to designers and enables the fabrication of multi-functional parts that are not possible to create with conventional manufacturing processes today. Multi-material 3D printing is only a budding technology, but will certainly lead to increasingly functional designs. Gaynor *et al.* [8] realized compliant mechanism designs based on three-phase [9, 10, 11] topology optimization using the PolyJet additive manufacturing technology, which can print bulk materials covering a wide range of elastic moduli [12]. Even using single material printers, functional designs have been fabricated by varying the microstructure throughout the print to achieve varying elastic properties [13]. Although the ability to control material properties at the voxel level is attractive, it also presents risk and uncertainty since defects can subsequently be introduced at similar scales. Thus, novel uncertainty aware synthesis optimization tools are needed to aid designers explore this new multi-material design space and insure designs against the inherent imperfections that multi-material 3D printers can facilitate.

This work aims to apply SROMs to account for the uncertainty in the orientation of an applied load and elastic modulus of the compliant material while solving a multi-material structural topology optimization problem under uncertainty. An SROM is a low-dimensional, discrete approximation to a continuous random element comprised of a finite and usually small number of samples with varying probabilities. This non-intrusive approach enables efficient stochastic computations in terms of only a small set of samples and probabilities. The SROM concept was originally proposed in [14] and then further refined in [15]. The SROM approach has been demonstrated in multiple applications, including the determination of effective conductivities for random microstructures [16], the estimation of linear dynamic system states [17, 18], inverse problems under uncertainty [19], the quantification of uncertainty in intergranular corrosion rates [20], and the prediction of the structural reliability of components containing laser welds [21]. The primary strengths of SROMs are their ability to represent an underlying random quantity with low-dimensionality and to subsequently solve uncertainty propagation problems in a fraction of the computational time required by Monte Carlo methods.

This work, to the best of our knowledge, represents the first application of SROMs to multi-material structural topology optimization under uncertainty. The SROM framework represents a practical approach with the following strengths shown in this work: 1) it relies entirely on calls to existing deterministic solvers and optimization libraries, 2) it is easily parallelized and scalable, and 3) it is not specific to normally distributed random quantities. Additionally, SROMs give higher weight to important areas of the probability space [19]. This property yields low-dimensional approximations and thus relatively few calls to deterministic models.

Formulation

First, let $H = L^2(\Omega;\mathbb{R}^d)$ denote the Hilbert space of measurable and square intregrable functions endowed with inner product $\langle \phi, \psi \rangle_H = \int_\Omega \phi\, \psi$ for $\phi, \psi \in H$ and norm $\|\phi\|_H = \langle \phi, \phi \rangle_H^{1/2}$. Additionally, the Sobolev space, H^1, is the set of all functions $\phi \in H$ such that every multi-index α with $|\alpha| \leq a$, the mixed partial derivative $D^\alpha \phi = \partial^{|\alpha|}\phi / \partial^{\alpha_1}\boldsymbol{x}_1^{\alpha_1} \cdots \partial^{\alpha_1}\boldsymbol{x}_n^{\alpha_n}$ exists in the weak sense, where $a = 1$. The Sobolev space H^1 is endowed with inner product $\langle \phi, \psi \rangle_{H^1} = \sum_{i=0}^{a} \langle D^i\phi, D^i\psi \rangle_H$ and norm $\|\phi\|_{H^1} = \sum_{i=1}^{a} \|D^i\phi\|_H$. Now, define the finite dimensional spaces $\mathbb{U} := \text{span}\{\phi_\mathsf{i}\}$, $\phi_\mathsf{i} \in H^1$ for $\mathsf{i} = 1, \ldots \mathsf{I}$, $\mathsf{I} \in \mathbb{N}$, $\mathbb{Y} := \text{span}\{\psi_\mathsf{j}\}$, $\psi_\mathsf{j} \in L^2(\Omega)$ for $\mathsf{j} = 1, \ldots \mathsf{J}$, $\mathsf{J} \in \mathbb{N}$, and $\mathbb{V}_\mathsf{i} = \text{span}\{\varphi_\mathsf{k}\}$, $\varphi_\mathsf{k} \in H^1$ for $\mathsf{k} = 1, \ldots \mathsf{K}$, $\mathsf{K} \in \mathbb{N}$. The finite dimensional approximations for the displacements, control points, and Lagrange multipliers can then be defined as $\boldsymbol{u} = \sum_{\mathsf{i}=1}^{\mathsf{I}} \hat{a}_\mathsf{i}\phi_\mathsf{i}$, $\hat{a}_\mathsf{i} \in \mathbb{R}\ \forall\ \mathsf{i} = 1, \ldots \mathsf{I}$, $\boldsymbol{x} = \sum_{\mathsf{j}=1}^{\mathsf{J}} \hat{b}_\mathsf{j}\psi_\mathsf{j}$, $\hat{b}_\mathsf{j} \in \mathbb{R}\ \forall\ \mathsf{j} = 1, \ldots \mathsf{J}$, and $\boldsymbol{\lambda} = \sum_{\mathsf{k}=1}^{\mathsf{K}} \hat{c}_\mathsf{k}\varphi_\mathsf{k}$, $\hat{c}_\mathsf{k} \in \mathbb{R}\ \forall\ \mathsf{k} = 1, \ldots \mathsf{K}$, respectively. The subsequent derivations will be based on the mathematical preliminaries presented above.

Governing linear elastostatic equation

A multi-material structural topology optimization problem in linear elastostatics seeks to find the set of material points $\boldsymbol{\omega} = \{\boldsymbol{x} \in \mathbb{R}^d\} \subset \Omega \subseteq \mathbb{R}^d$ and the spatial distribution of material tensor $D(\boldsymbol{x})$ such that an objective function is extremized, an arbitrary constraint (or set of constraints) is satisfied, and the displacement field $\boldsymbol{u} \in \mathscr{U}$ satisfies the governing equations

$$\int_{\boldsymbol{\omega}} D(\boldsymbol{x})\nabla\boldsymbol{u} \colon \nabla\boldsymbol{\delta u}\, d\boldsymbol{\omega} = \int_{\Gamma_t} t \cdot \boldsymbol{\delta u}\, d\Gamma_t \quad \forall\ \boldsymbol{\delta u} \in \mathscr{U}_0. \tag{4}$$

In Equation (4), Ω denotes the computational domain with spatial dimension d and boundary $\Gamma = \Gamma_u \cup \Gamma_t,\ \Gamma_u \cap \Gamma_t = \emptyset$. The set of control points $\boldsymbol{\omega}$ defines the optimal geometry, $\mathscr{U} = \{\boldsymbol{u} \in H^1 \colon \boldsymbol{u} = \boldsymbol{u}_0 \text{ on } \Gamma_{\boldsymbol{u}}\}$ is the set of trial functions, $\boldsymbol{u}_0$ is the set of prescribed displacements (Dirichlet conditions), $\mathscr{U}_0 = \{\delta\boldsymbol{u} \in H^1 \colon \delta\boldsymbol{u} = 0 \text{ on } \Gamma_{\boldsymbol{u}}\}$ is the set of test functions, $\Gamma_u \subset \Gamma$ is the portion of the boundary were Dirichlet conditions are prescribed, and Γ_t is the portion of the boundary where surface tractions are applied (Neumann conditions).

The optimal set of control points are defined by an indicator function $\chi_\omega(\boldsymbol{x})$ defined as

$$\chi_\omega(\boldsymbol{x}) = \begin{cases} 1 & \text{if} \quad \boldsymbol{x} \in \boldsymbol{\omega} \\ 0 & \text{if} \quad \boldsymbol{x} \in \Omega \setminus \boldsymbol{\omega} \end{cases} . \tag{5}$$

The spatial distribution of material tensor $D(\boldsymbol{x})$ is selected from a finite set of candidate material tensors at each control point such that

$$D(\boldsymbol{x}) = \phi(\mathscr{D}), \tag{6}$$

where $\mathscr{D} = \{D_m(\boldsymbol{x})\}_{m=1}^M$ is the set of candidate material tensors at control point $\boldsymbol{x}$ and ϕ is a choice function for which $\phi(\mathscr{D}) \in \mathscr{D}$ holds. With Equations (5) and (6) defined, Equation (4) is recast as

$$\int_\Omega (\chi_\omega(\boldsymbol{x})\phi(\mathscr{D}))\nabla\boldsymbol{u} \colon \nabla\delta\boldsymbol{u}\, d\Omega = \int_{\Gamma_t} t \cdot \delta\boldsymbol{u}\, d\Gamma_t \quad \forall\ \delta\boldsymbol{u} \in \mathscr{U}_0. \tag{7}$$

Equation (7) is impractical to consider for multi-material structural topology optimization since finding $\boldsymbol{\omega}$ and $D(\mathbf{x})$ becomes a large-scale integer programming problem. Therefore, $\chi_\omega(\boldsymbol{x})$ and $\phi(\mathscr{D})$ are recast as a set of m continuous material density fields defined as $\mathscr{P} = \{\rho_m\}_{m=1}^M$, where $\rho_m \in L^2(\Omega)$ and $\rho_m(\boldsymbol{x}) \in [0,1]$. The total density (i.e. volume fraction) at control point $\boldsymbol{x}$ is defined as $\rho_T(\boldsymbol{x}) = \sum_{m=1}^M \rho_m(\boldsymbol{x})$. The magnitude of ρ_T is used to determine the contribution of each candidate material at control point $\boldsymbol{x}$ according to a Discrete Material Optimization (DMO) interpolation function, $\beta(\boldsymbol{x}) = \eta(\rho_m(\boldsymbol{x}), D_m(\boldsymbol{x}))$, where $\beta \in \mathbb{R}$. The DMO interpolation function aims to improve the approximation of the integer programming problem and discourage material mixing [22, 23]. In this work a summation interpolation rule is used as the DMO interpolation function [24, 25]. Thus, (7) is recast as

$$\int_\Omega \eta(\rho_m(\boldsymbol{x}), D_m(\boldsymbol{x}))\nabla\boldsymbol{u} \colon \nabla\delta\boldsymbol{u}\, d\Omega = \int_{\Gamma_t} t \cdot \delta\boldsymbol{u}\, d\Gamma_t \quad \forall\ \delta\boldsymbol{u} \in \mathscr{U}_0, \text{ for } m = 1, \ldots M. \tag{8}$$

Note that the formulation in (8) enables the use of gradient-based optimization algorithms.

To avoid the numerical artifacts (e.g. checkerboard patterns) [26, 27] that may result from the discretization of the candidate density fields due to unstable finite element formulations, each candidate density field is filtered by convolution as follows

$$\hat{\rho}_m(\boldsymbol{x}) = (F * \rho_m)(\boldsymbol{x}) = \int_{B_R} F(\boldsymbol{x}, \boldsymbol{y})\rho_m(\boldsymbol{x})\, d\boldsymbol{y}. \tag{9}$$

In Equation (9), $\hat{\rho}_m(\boldsymbol{x})$ is the filtered density field for candidate material m, $\boldsymbol{y} \in \Omega$, and B_R is the ball of radius R that defines the radius of influence. The material interpolation function in (8) can

be re-written in terms of the m candidate filtered density fields from (9). Therefore, the governing linear elastostatic equation becomes

$$\int_{\Omega} \eta(\hat{\rho}_m(\boldsymbol{x}), D_m(\boldsymbol{x}))\nabla \boldsymbol{u} \colon \nabla \delta \boldsymbol{u}\, d\Omega = \int_{\Gamma_t} t \cdot \delta \boldsymbol{u}\, d\Gamma_t \quad \forall\, \delta \boldsymbol{u} \in \mathscr{U}_0, \text{ for } m = 1, \ldots M. \tag{10}$$

Deterministic multi-material structural topology optimization

After applying the finite element method [28] to (10) and discretizing the computational domain into finite elements, a multi-material structural topology optimization problem based on the Solid Isotropic Material with Penalization (SIMP) [29, 30] approach can be written as

$$\begin{aligned} \mathscr{X}^* = \arg\min_{\mathscr{X}} :\ & C(\widehat{\mathscr{X}}) = \boldsymbol{u}^T[\boldsymbol{k}(\widehat{\mathscr{X}}, \mathscr{E})]\boldsymbol{u} = \sum_{m=1}^{M}\sum_{e=1}^{N_e} (z_m^e(\hat{\boldsymbol{x}}_m^k))^{\mu} \boldsymbol{u}_e^T[\boldsymbol{k}_e(\boldsymbol{\varepsilon}_m)]\boldsymbol{u}_e \\ \text{subject to} :\ & \boldsymbol{r}(\boldsymbol{u}, \widehat{\mathscr{X}}, \mathscr{E}; \vartheta) = \boldsymbol{0} \quad \text{in} \quad \Omega \\ :\ & \sum_{m=1}^{M}\sum_{e=1}^{N_e} z_m^e(\hat{x}_m^k)\gamma_m V_e \leq \mathrm{M}_{\max} \\ :\ & \boldsymbol{0} \leq \boldsymbol{x}_m \leq \boldsymbol{1}, \end{aligned} \tag{11}$$

where

$$\boldsymbol{r}(\boldsymbol{u}, \widehat{\mathscr{X}}, \mathscr{E}; \vartheta) = [\boldsymbol{k}(\widehat{\mathscr{X}}, \mathscr{E})]\boldsymbol{u} - \boldsymbol{f}(\vartheta) \tag{12}$$

is the deterministic residual equation. In Equation (11), $\boldsymbol{\varepsilon}_m$ is the elastic modulus for candidate material m and $\mathscr{E} = \{\boldsymbol{\varepsilon}_m\}_{m=1}^{M}$ is the set of elastic moduli, $[\boldsymbol{k}]$ is the global deterministic stiffness matrix and $[\boldsymbol{k}_e]$ is the deterministic element stiffness matrix, $\boldsymbol{u}$ is the global deterministic displacement vector, and $\boldsymbol{f}$ is the global deterministic force vector resulting from an applied load with orientation ϑ.

A kernel filter was used to avoid numerical artifacts that may result from the discretization of the control points with possibly unstable finite element formulations. Specifically, a linear kernel filter [31, 32]

$$F_{ik} = \max\left(0, 1 - \frac{d(i,k)}{R}\right) \tag{13}$$

is applied to the control points to avoid the aforementioned numerical artifacts. Therefore, the filtered control points $\hat{\boldsymbol{x}}_m^k$ for candidate material m are given by

$$\hat{\boldsymbol{x}}_m^k = \sum_{i=1} = w^{ik}\boldsymbol{x}_m^i, \tag{14}$$

where the weights in (14) are defined as

$$w^{ik} = \frac{F_{ik}}{\sum_{l \in \mathscr{N}_k} F_{lk}}. \tag{15}$$

In Equations (13)-(15), $d(i,k)$ is the distance between control points $\boldsymbol{x}_m^i$ and $\boldsymbol{x}_m^k$ for candidate material m and R is the filter's radius of influence. $\mathscr{N}_k = \{\boldsymbol{x}_m^i \colon d(i,k) \leq R\}$ is the neighborhood

of control points that are inside the radius R, including the control points on the boundary of the radius, with respect to control point $\boldsymbol{x}_m^k$.

Generic Description of SROM

An SROM is a discrete approximation of a random quantity (variable, vector, etc.) defined by a finite and generally small number of samples with varying probability. In this work, an SROM $\tilde{\Theta}$ defined by parameters $\{\tilde{\theta}^{(\mathrm{u})}, p_\theta^{(\mathrm{u})}\}_{\mathrm{u}=1}^{\mathrm{s}_\theta}$, is used as low dimensional approximations of random parameter Θ. The SROM $\tilde{\Theta}$ has size s_θ with samples $\{\tilde{\theta}^{(\mathrm{u})}\}_{\mathrm{u}=1}^{\mathrm{s}_\theta}$ and probabilities $\boldsymbol{p}_\theta = (p_\theta^{(\mathrm{u})}, \ldots, p_\theta^{(\mathrm{s}_\theta)})$ associated with each sample, where $p_\theta^{(\mathrm{u})} \geq 0 \; \forall \, \mathrm{u} = 1, \ldots, \mathrm{s}_\theta$, $\mathrm{s}_\theta \in \mathbb{N}$, and $\sum_{\mathrm{u}=1}^{\mathrm{s}_\theta} p_\theta^{(\mathrm{u})} = 1$. The cumulative distribution function (CDF) of the SROM $\tilde{\Theta}$ is expressed as

$$\begin{aligned} \tilde{F}(\theta) &= P(\tilde{\Theta} \leq \theta) \\ &= \sum_{\mathrm{u}=1}^{\mathrm{s}_\theta} p_\theta^{(\mathrm{u})} \mathbf{1}_{\tilde{\Theta}} \left(\tilde{\theta}^{(\mathrm{u})} \leq \theta \right), \end{aligned} \tag{16}$$

where $\mathbf{1}_{\tilde{\Theta}}(\tilde{\theta}^{(\mathrm{u})} \leq \theta)$ is an indicator function defined as

$$\mathbf{1}_{\tilde{\Theta}}(\tilde{\theta}^{(\mathrm{u})} \leq \theta) := \begin{cases} 1 & \text{if } \tilde{\theta}^{(\mathrm{u})} \leq \theta \\ 0 & \text{if } \tilde{\theta}^{(\mathrm{u})} > \theta \end{cases}, \tag{17}$$

while q^{th} order moments are given by

$$\begin{aligned} \tilde{\mu}(q) &= E\left[\tilde{\Theta}^q\right] \\ &= \sum_{\mathrm{u}=1}^{\mathrm{s}_\theta} p_\theta^{(\mathrm{u})} (\tilde{\theta}^{(\mathrm{u})})^q. \end{aligned} \tag{18}$$

The SROM, $\tilde{\Theta}$, is constructed such that it approximates Θ as best as possible in a statistical sense. For a given random variable, Θ, with known CDF, $F(\theta)$, and moments, $\mu(q)$, this is done by selecting the defining SROM parameters through the following optimization problem

$$\begin{aligned} \tilde{\Theta} := \underset{\{\tilde{\theta}\}, \boldsymbol{p}_\theta}{\operatorname{argmin}} & \left(\alpha_1 \int_{I_\theta} \left(\tilde{F}(\theta) - F(\theta) \right)^2 d\theta + \alpha_2 \sum_{q=1}^{\bar{q}} \left(\frac{(\tilde{\mu}(q) - \mu(q))}{\mu(q)} \right)^2 \right) \\ \text{subject to} : & \sum_{\mathrm{u}=1}^{\mathrm{s}_\theta} p_\theta^{(\mathrm{u})} = 1 \text{ and } p_\theta^{(\mathrm{u})} \geq 0 \; \forall \, \mathrm{u} = 1, ..., \mathrm{s}_\theta. \end{aligned} \tag{19}$$

In Equation (19), α_1 is the weighting factor controlling the relative importance of matching the target CDF, α_2 is the weighting factor controlling the relative importance of matching the moments up to order $\bar{q}$, and $\int_{I_\theta}$ is the support of Θ. More details on the solution of (19) can be found in [15].

Multiple sources of uncertainty with SROMs

An additional strength of the SROM approach is that it can be naturally extended to handle problems with multiple sources of uncertainty. Consider the case where, in addition to the parameter Θ, the state solution, $\boldsymbol{U}$, also depends on a separate and independent source of randomness

represented by the random element Σ. This could occur, for example, when the variability in the state is influenced by both internal randomness (e.g. material properties) as well as uncertainty from external sources (e.g. applied load). In this case, the residual equation takes the form of (3), where Σ is the random elastic modulus of the compliant material and Θ is the random orientation of the applied load. Note that the random parameters could be encapsulated as $\boldsymbol{Y} := [\Theta\ \Sigma]$, which enables to use a single random parametric representation in (3). However, for convenience, we will not use the encapsulation of the random parameters, $\boldsymbol{Y}$, in the subsequent derivations.

The procedure for solving (3) using multiple SROMs is consistent with the approach described previously for Θ with the caveat of treating the additional random element Σ. The SROMs $\tilde{\Theta} := \{\tilde{\theta}^{(\mathrm{u})}, p_{\theta}^{(\mathrm{u})}\}_{\mathrm{u}=1}^{\mathrm{s}_\theta}$ and $\tilde{\Sigma} := \{\tilde{\varepsilon}^{(\mathrm{v})}, p_{\varepsilon}^{(\mathrm{v})}\}_{\mathrm{v}=1}^{\mathrm{s}_\varepsilon}$ must be respectively formed in this case for both Θ and Σ by solving the optimization problem in (19) given the probabilistic description of each random parameter. Therefore, after the SROM $\tilde{\Theta}$ and $\tilde{\Sigma}$ have been determined through (19), these SROMs can be used to efficiently and non-intrusively propagate uncertainty through (3). In a manner analogous to Monte Carlo methods, this is done by evaluating the deterministic model in (12) $\mathrm{s}_{\boldsymbol{u}} = \mathrm{s}_\varepsilon \times \mathrm{s}_\theta$ times as

$$\boldsymbol{R}(\tilde{\boldsymbol{u}}^{(\mathrm{w})}, \widehat{\mathscr{X}}, \tilde{\varepsilon}^{(\mathrm{v})}; \tilde{\theta}^{(\mathrm{u})}) = \boldsymbol{0}, \quad \mathrm{u} = 1, \ldots, \mathrm{s}_\theta, \quad \mathrm{v} = 1, \ldots, \mathrm{s}_\varepsilon, \tag{20}$$

where $\mathrm{w} = (\mathrm{v}-1) \times \mathrm{s}_\varepsilon + \mathrm{u}$, $\mathrm{s}_\varepsilon \in \mathbb{N}$ is the size of SROM $\tilde{\Sigma}$, and $\mathrm{s}_{\boldsymbol{u}} \in \mathbb{N}$ is the size of SROM $\tilde{\boldsymbol{U}}$. The resulting set of state samples, $\{\tilde{\boldsymbol{u}}^{(\mathrm{w})}\}_{\mathrm{w}=1}^{\mathrm{s}_{\boldsymbol{u}}}$ and probabilities $p_{\boldsymbol{u}}^{(\mathrm{w})} = p_\theta^{(\mathrm{u})} \times p_\varepsilon^{(\mathrm{v})}$ define an SROM $\tilde{\boldsymbol{U}}$ for random vector $\boldsymbol{U}$. The statistics of $\boldsymbol{U}$ can then be estimated using the analogous multidimensional versions of Equations (16) and (18). It has been shown in previous work [15, 20] that the number of model evaluations, $\mathrm{s}_{\boldsymbol{u}}$, required by SROMs can be substantially less than traditional Monte Carlo while retaining similar accuracy. In this way, SROMs can be viewed as a smart Monte Carlo method, where preprocessing is done through the optimization problem in (19) to yield a set, or sets, of probabilities that are tuned to best reflect the original statistics of the random inputs.

Multi-matrial structural topology optimization using SROMs

Lets consider an uncertainty aware, multi-material, structural topology optimization problem where the number of candidate materials is set to two ($M = 2$), the stiffer material properties are considered known and deterministic, and the randomness in the model is introduced through uncertainty in the elastic modulus of the compliant material and the orientation of the applied load. The SROMs $\tilde{\Theta}$ and $\tilde{\Sigma}$ are first generated by solving (19) and optimizing for the defining SROM parameters $\{\tilde{\theta}^{(\mathrm{u})}, p_\theta^{(\mathrm{u})}\}_{\mathrm{u}=1}^{\mathrm{s}_\theta}$ and $\{\tilde{\varepsilon}^{(\mathrm{v})}, p_\varepsilon^{(\mathrm{v})}\}_{\mathrm{v}=1}^{\mathrm{s}_\varepsilon}$, respectively. The parameterization of the random direction, Θ, and elastic modulus, Σ, via SROM enables us to recast (1) as

$$\begin{aligned}\mathscr{X}^* = \underset{\mathscr{X}}{\arg\min}: \ \tilde{C}(\widehat{\mathscr{X}}) &= E\left[\boldsymbol{U}^T[\boldsymbol{K}(\widehat{\mathscr{X}}, \tilde{\Sigma})]\boldsymbol{U}\right] = \sum_{v=1}^{\mathrm{s}_\varepsilon}\sum_{u=1}^{\mathrm{s}_\theta} p_\varepsilon^{(\mathrm{v})} p_\theta^{(\mathrm{u})} (\tilde{\boldsymbol{u}}^{(\mathrm{w})})^T [\boldsymbol{K}(\widehat{\mathscr{X}}, \tilde{\varepsilon}^{(\hat{\mathrm{v}})})]\tilde{\boldsymbol{u}}^{(\mathrm{w})} \\ &= \sum_{v=1}^{\mathrm{s}_\varepsilon}\sum_{u=1}^{\mathrm{s}_\theta} p_\varepsilon^{(\mathrm{v})} p_\theta^{(\mathrm{u})} \sum_{m=1}^{M}\sum_{e=1}^{N} (z_m^e(\hat{\boldsymbol{x}}_m^k))^\mu (\tilde{\boldsymbol{u}}_e^{(\mathrm{w})})^T [\boldsymbol{k}_e(\tilde{\boldsymbol{\varepsilon}}^{(\hat{\mathrm{v}})})]\tilde{\boldsymbol{u}}_e^{(\mathrm{w})}\end{aligned}$$

$$
\begin{aligned}
\text{subject to} \;:\; & \boldsymbol{R}(\tilde{\boldsymbol{u}}^{(\mathrm{w})}, \widehat{\mathscr{X}}, \tilde{\boldsymbol{\varepsilon}}^{(\hat{\mathrm{v}})}; \tilde{\boldsymbol{\theta}}^{(\mathrm{u})}) = \boldsymbol{0} \quad \text{in} \quad \Omega \quad \text{a.s., for } \mathrm{w} = (\mathrm{v}-1)\times s_{\boldsymbol{\varepsilon}} + \mathrm{u} \\
: \; & \sum_{m=1}^{M} \sum_{e=1}^{N_e} z_m^e(\hat{x}_m^k)\gamma_m V_e \leq \mathrm{M}_{\max} \\
: \; & \boldsymbol{0} \leq \boldsymbol{x}_m \leq \boldsymbol{1},
\end{aligned}
\tag{21}
$$

where

$$
\boldsymbol{R}(\tilde{\boldsymbol{u}}^{(\mathrm{w})}, \widehat{\mathscr{X}}, \tilde{\boldsymbol{\varepsilon}}^{(\hat{\mathrm{v}})}; \tilde{\boldsymbol{\theta}}^{(\mathrm{u})}) = [\boldsymbol{K}(\widehat{\mathscr{X}}, \tilde{\boldsymbol{\varepsilon}}^{(\hat{\mathrm{v}})})]\tilde{\boldsymbol{u}}^{(\mathrm{w})} - \boldsymbol{F}(\tilde{\boldsymbol{\theta}}^{(\mathrm{u})}). \tag{22}
$$

In Equations (21) and (22), $\hat{\mathrm{v}} = \mathrm{v} \times (m-1) + 1$, where the first entry of the set of elastic moduli is reserved for the deterministic candidate material. Note that the stochastic algebraic constraint in (22) has been transformed into a set of $\mathrm{s}_{\boldsymbol{u}}$ independent deterministic constraint equations using the SROM. The decoupling of these equations allows them to be evaluated in parallel with simultaneous calls to the original deterministic analysis software.

Gradient Derivation

The adjoint approach based on a Lagrangian formulation was used to derive the gradient of the objective function in (21) with respect to the set of control points $\mathscr{X}$. Lets assume that the objective function in (21) is differentiable with respect to the m candidate control points $\boldsymbol{x}_m$ and that the formulation is based on nodal control points. Then, the Lagrangian function for (21) is defined as

$$
\mathscr{L}(\widehat{\mathscr{X}}, \tilde{\boldsymbol{\lambda}}^{(\mathrm{w})}) := \tilde{C}(\widehat{\mathscr{X}}) + (\tilde{\boldsymbol{\lambda}}^{(\mathrm{w})})^T([\boldsymbol{K}(\widehat{\mathscr{X}}, \tilde{\boldsymbol{\varepsilon}}^{(\hat{\mathrm{v}})})]\tilde{\boldsymbol{u}}^{(\mathrm{w})} - \boldsymbol{F}(\tilde{\boldsymbol{\theta}}^{(\mathrm{u})})), \text{ for } \mathrm{w} = (\mathrm{v}-1)\times s_{\boldsymbol{\varepsilon}} + \mathrm{u}, \tag{23}
$$

where $\tilde{\boldsymbol{\lambda}}^{(\mathrm{w})} \in \mathbb{R}^{\mathrm{N}\lambda}$ denotes the w-th sample of the vector of Lagrange multipliers and N_λ is the total number of Lagrange multipliers. Since $\boldsymbol{R}(\boldsymbol{u}^{(\mathrm{w})}, \widehat{\mathscr{X}}, \tilde{\boldsymbol{\varepsilon}}^{(\hat{\mathrm{v}})}; \tilde{\boldsymbol{\theta}}^{(\mathrm{u})}) = 0$ is satisfied for all choices of $\tilde{\boldsymbol{\lambda}}^{(\mathrm{w})}$, the gradient of the objective function with respect to the m control points, $\boldsymbol{x}_m$, is given by $\frac{d\mathscr{L}}{d\boldsymbol{x}_m}$. Therefore, by using the fact that the displacement samples, $\{\tilde{\boldsymbol{u}}^{(\mathrm{w})}\}_{\mathrm{w}=1}^{\mathrm{s}_{\boldsymbol{u}}}$, are viewed as implicit functions of $\boldsymbol{x}_m$, the derivative of (23) with respect to the m control points is given by

$$
\begin{aligned}
\frac{d\mathscr{L}(\widehat{\mathscr{X}}, \tilde{\boldsymbol{\lambda}}^{(\mathrm{w})})}{d\boldsymbol{x}_m^k} &= \frac{\partial \tilde{C}(\widehat{\mathscr{X}})}{\partial z_m^e}\frac{\partial z_m^e}{\partial \hat{\boldsymbol{x}}_m^k}\frac{\partial \hat{\boldsymbol{x}}_m^k}{\partial \boldsymbol{x}_m^k} + \frac{\partial \tilde{C}(\widehat{\mathscr{X}})}{\partial \tilde{\boldsymbol{u}}_e^{(\mathrm{w})}}\frac{\partial \tilde{\boldsymbol{u}}_e^{(\mathrm{w})}}{\partial \boldsymbol{x}_m^k} \\
&+ (\tilde{\boldsymbol{\lambda}}_e^{(\mathrm{w})})^T\left(\frac{\partial R(\tilde{\boldsymbol{u}}^{(\mathrm{w})}, \widehat{\mathscr{X}}, \tilde{\boldsymbol{\varepsilon}}^{(\hat{\mathrm{v}})}; \tilde{\boldsymbol{\theta}}^{(\mathrm{u})})}{\partial z_m^e}\frac{\partial z_m^e}{\partial \hat{\boldsymbol{x}}_m^k}\frac{\partial \hat{\boldsymbol{x}}_m^k}{\partial \boldsymbol{x}_m^k} + \frac{\partial R(\tilde{\boldsymbol{u}}^{(\mathrm{w})}, \widehat{\mathscr{X}}, \tilde{\boldsymbol{\varepsilon}}^{(\hat{\mathrm{v}})}; \tilde{\boldsymbol{\theta}}^{(\mathrm{u})})}{\partial \tilde{\boldsymbol{u}}_e^{(\mathrm{w})}}\frac{\partial \tilde{\boldsymbol{u}}_e^{(\mathrm{w})}}{\partial \boldsymbol{x}_m^k}\right),
\end{aligned}
\tag{24}
$$

where (24) is explicitly expressed as

$$
\begin{aligned}
&\sum_{\mathrm{v}=1}^{\mathrm{s}_{\boldsymbol{\varepsilon}}}\sum_{\mathrm{u}=1}^{\mathrm{s}_{\boldsymbol{\theta}}}\Bigg(p_{\boldsymbol{\varepsilon}}^{(\mathrm{v})}p_{\boldsymbol{\theta}}^{(\mathrm{u})}\Bigg(\mu(z_m^e(\hat{\boldsymbol{x}}_m^k))^{\mu-1}\frac{\partial z_m^e}{\partial \hat{\boldsymbol{x}}_m^k}\frac{\partial \hat{\boldsymbol{x}}_m^k}{\partial \boldsymbol{x}_m^k}(\tilde{\boldsymbol{u}}_e^{(\mathrm{w})})^T[\boldsymbol{k}_e(\tilde{\boldsymbol{\varepsilon}}^{(\hat{\mathrm{v}})})]\tilde{\boldsymbol{u}}_e^{(\mathrm{w})} \\
&\quad + (\tilde{\boldsymbol{\lambda}}_e^{(\mathrm{w})})^T\left(\mu(z_m^e(\hat{\boldsymbol{x}}_m^k))^{\mu-1}\frac{\partial z_m^e}{\partial \hat{\boldsymbol{x}}_m^k}\frac{\partial \hat{\boldsymbol{x}}_m^k}{\partial \boldsymbol{x}_m^k}[\boldsymbol{k}_e(\tilde{\boldsymbol{\varepsilon}}^{(\hat{\mathrm{v}})})]\tilde{\boldsymbol{u}}_e^{(\mathrm{w})}\right)\Bigg) \\
&\quad + \left(p_{\boldsymbol{\varepsilon}}^{(\mathrm{v})}p_{\boldsymbol{\theta}}^{(\mathrm{u})}\left(2(z_m^e(\hat{\boldsymbol{x}}_m^k))^{\mu}[\boldsymbol{k}_e(\tilde{\boldsymbol{\varepsilon}}^{(\hat{\mathrm{v}})})]\tilde{\boldsymbol{u}}_e^{(\mathrm{w})}\right) + (\tilde{\boldsymbol{\lambda}}_e^{(\mathrm{w})})^T(z_m^e(\hat{\boldsymbol{x}}_m^k))^{\mu}[\boldsymbol{k}_e(\tilde{\boldsymbol{\varepsilon}}^{(\hat{\mathrm{v}})})]\right)\frac{\partial \tilde{\boldsymbol{u}}_e^{(\mathrm{w})}}{\partial \boldsymbol{x}_m^k}\Bigg).
\end{aligned}
\tag{25}
$$

Since the the adjoint method is being applied to derive the gradient of (21), the third term in (25) is eliminated by choosing the Lagrange multipliers such that they satisfy

$$(z_m^e(\hat{\boldsymbol{x}}_m^k))^\mu [\boldsymbol{k}_e(\tilde{\boldsymbol{\varepsilon}}^{(\hat{\mathrm{v}})})]^T \tilde{\boldsymbol{\lambda}}_e^{(\mathrm{w})} = -p_\varepsilon^{(\mathrm{v})} p_\theta^{(\mathrm{u})} \left(2(z_m^e(\hat{\boldsymbol{x}}_m^k))^\mu [\boldsymbol{k}_e(\tilde{\boldsymbol{\varepsilon}}^{(\hat{\mathrm{v}})})] \tilde{\boldsymbol{u}}_e^{(\mathrm{w})} \right). \tag{26}$$

Therefore, the gradient of (23) is recast as

$$\begin{aligned} \sum_{\mathrm{v}=1}^{\mathrm{s}_\varepsilon} \sum_{\mathrm{u}=1}^{\mathrm{s}_\theta} \Bigg(p_\varepsilon^{(\mathrm{v})} p_\theta^{(\mathrm{u})} \Bigg(\mu (z_m^e(\hat{\boldsymbol{x}}_m^k))^{\mu-1} \frac{\partial z_m^e}{\partial \hat{\boldsymbol{x}}_m^k} \frac{\partial \hat{\boldsymbol{x}}_m^k}{\partial \boldsymbol{x}_m^k} (\tilde{\boldsymbol{u}}_e^{(\mathrm{w})})^T [\boldsymbol{k}_e(\tilde{\boldsymbol{\varepsilon}}^{(\hat{\mathrm{v}})})] \tilde{\boldsymbol{u}}_e^{(\mathrm{w})} \Bigg) \\ + (\tilde{\boldsymbol{\lambda}}_e^{(j)})^T \Bigg(\mu (z_m^e(\hat{\boldsymbol{x}}_m^k))^{\mu-1} \frac{\partial z_m^e}{\partial \hat{\boldsymbol{x}}_m^k} \frac{\partial \hat{\boldsymbol{x}}_m^k}{\partial \boldsymbol{x}_m^k} [\boldsymbol{k}_e(\tilde{\boldsymbol{\varepsilon}}^{(\hat{\mathrm{v}})})] \tilde{\boldsymbol{u}}_e^{(\mathrm{w})} \Bigg) \Bigg). \end{aligned} \tag{27}$$

Since $[\boldsymbol{k}_e]$ is self-adjoint and non-singular, the Lagrange multipliers can be explicitly expressed as

$$\tilde{\boldsymbol{\lambda}}_e^{(\mathrm{w})} = -2 p_\varepsilon^{(\mathrm{v})} p_\theta^{(\mathrm{u})} \tilde{\boldsymbol{u}}_e^{(\mathrm{w})}. \tag{28}$$

Next, Equation (28) is plugged into (27), which enables Equation (27) to be recast as

$$\sum_{\mathrm{v}=1}^{\mathrm{s}_\varepsilon} \sum_{\mathrm{u}=1}^{\mathrm{s}_\theta} \left(-p_\varepsilon^{(\mathrm{v})} p_\theta^{(\mathrm{u})} \left(\mu (z_m^e(\hat{\boldsymbol{x}}_m^k))^{\mu-1} \frac{\partial z_m^e}{\partial \hat{\boldsymbol{x}}_m^k} \frac{\partial \hat{\boldsymbol{x}}_m^k}{\partial \boldsymbol{x}_m^k} (\tilde{\boldsymbol{u}}_e^{(\mathrm{w})})^T [\boldsymbol{k}_e(\tilde{\boldsymbol{\varepsilon}}^{(\hat{\mathrm{v}})})] \tilde{\boldsymbol{u}}_e^{(\mathrm{w})} \right) \right). \tag{29}$$

Equation (29) yields the gradient of the objective function defined in (21).

Finally, the derivative of the mass or monetary constraint for candidate material m is defined as

$$\frac{\partial z_m^e(\hat{\boldsymbol{x}}_m^k)}{\partial \hat{\boldsymbol{x}}_m^k} \frac{\partial \hat{\boldsymbol{x}}_m^k}{\partial \boldsymbol{x}_m^k} \gamma_m V_e. \tag{30}$$

Note that $\partial z_m^e(\hat{\boldsymbol{x}}_m^k)/\partial \hat{\boldsymbol{x}}_m^k = 1$ if element control points are used instead of nodal control points. Furthermore, $\partial \hat{\boldsymbol{x}}_m^k / \partial \boldsymbol{x}_m^k$ will depend on the type of kernel filter used to solve (21).

The sequence of steps for computing the objective function and gradient for the uncertainty aware, multi-material, structural topology optimization problem defined in (21) are summarized next. After solving the optimization problem in (19) for the set of SROM parameters, $\{\tilde{\boldsymbol{\theta}}^{(\mathrm{u})}, p_\theta^{(\mathrm{u})}\}_{\mathrm{u}=1}^{\mathrm{s}_\theta}$ and $\{\tilde{\boldsymbol{\varepsilon}}^{(\mathrm{v})}, p_\varepsilon^{(\mathrm{v})}\}_{\mathrm{v}=1}^{\mathrm{s}_\varepsilon}$, the following procedure is repeated during optimization to compute the objective function and gradient of (21) at each iteration:

1. Solve $\mathrm{s}_{\boldsymbol{u}}$ decoupled, physics problems for the displacement samples, $\{\tilde{\boldsymbol{u}}^{(\mathrm{w})}\}_{\mathrm{w}=1}^{\mathrm{s}_{\boldsymbol{u}}}$, using (22).
2. Evaluate the expected value in the structural compliance, $\tilde{C}(\widehat{\mathscr{X}})$, defined in (21).
3. Compute the gradient of the objective function using (29).

Notice that computing the objective function and its gradient at each iteration require $\mathrm{s}_{\boldsymbol{u}}$ deterministic model evaluations. However, since the solves are decoupled and thus independent of each other, they can be easily parallelized and solved simultaneously to minimize computational cost. Furthermore, it is worth noting that the Hessian (or the application of the Hessian on a vector) can be easily derived along similar lines to the approach used for the deterministic case [33].

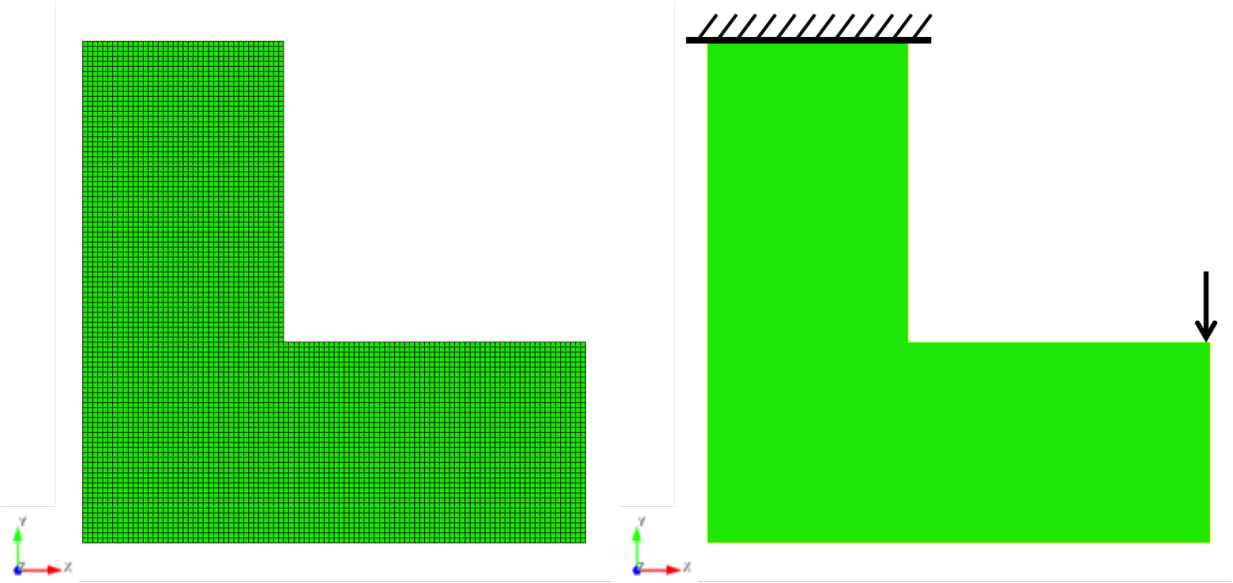

Figure 1: Problem domain used to solve the uncertainty aware, multi-material, structural topology optimization problem. The left pane shows the computational mesh. The right pane shows the isosurface and the corresponding boundary conditions used to solve the uncertainty aware, multi-material, structural topology optimization problem.

Numerical Examples

In this section, the SROM approach is used to solve a multi-material structural topology optimization problem where randomness is introduced through uncertainty in the orientation of the applied load and the elastic modulus of the compliant material. The SROM approach described in the previous section, Equation (19), was implemented using the optimization toolbox in MATLAB [34]. The implementation is based on the fmincon function for constrained nonlinear optimization. In all the examples presented herein, the interior-point algorithm was used along with a L-BFGS [35] Hessian approximation.

A sketch for the problem domain can be seen in Figure 1. Figure 1 shows that fixed boundary conditions were applied along the top surface of the allowable design domain, while a compressive force along the y-axis with magnitude of one was applied on the right-hand corner. The computational mesh with 6,400 four-node quadrilateral finite elements was created with Cubit [36]. The Intrepid partial differential equation (PDE) discretization package from Trilinos [37] was used to build the finite element model and the direct solver from MATLAB [34] was used to solve the finite element system of equations. The elastic modulus and Poisson's ratio for the stiff material were set to 1 and 0.3, respectively. The Poisson's ratio for the compliant material (soft material) was set to 0.3.

The SROM approach was used to solve (21) when considering randomness in the orientation of the applied load and the elastic modulus of the compliant material. The mass or monetary limit, M_{max}, was set to 0.4. The uncertainty in load orientation was modeled as a beta random variable with distribution, beta(2.1667,4.3333), on the interval $[67.5^\circ\ 135^\circ]$ while the uncertainty for the elastic moduli of the compliant material was modeled with distribution, beta(1.6250,4.8750), on the interval $[0.6\ 1.4]$. The stiff and soft candidate materials' mass density or cost, γ_m, were set

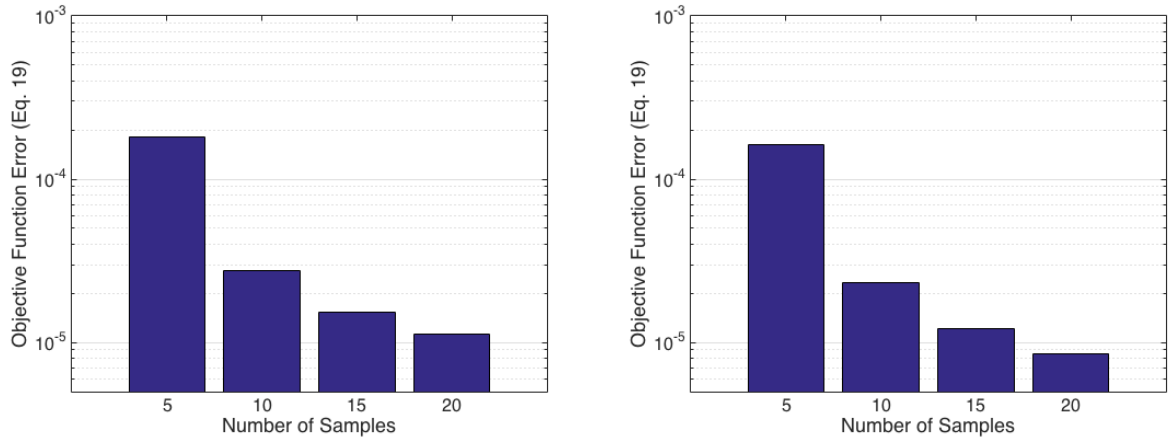

Figure 2: Convergence of the SROM construction problem (19) with increasing SROM size. The left pane shows the convergence for the SROM constructed for the random direction of the applied load, $\tilde{\Theta}$. The right pane shows the convergence for the SROM constructed for the random elastic modulus for the compliant material, $\tilde{\Sigma}$.

to 1 and 0.95, respectively. A MATLAB implementation of the globally convergent method of moving asymptotes (GCMMA) algorithm [38] implemented by the authors was used to solve (21). The algorithm was terminated based on a tolerance on the relative change in the solution between iterations or the maximum number of iterations, specified as $\varepsilon \leq 10^{-2}$ or 100, respectively. The initial guess for the set of control points, $\widehat{\mathscr{X}}$, were set to the target mass or monetary limit. The filter's radius of influence was set to two times the smallest element length, i.e. $R = 2\ell_e$.

The first step to solve (21) was to generate the SROMs $\tilde{\Theta}$ and $\tilde{\Sigma}$ for the random orientations of the applied load and the elastic modulus for the compliant material, respectively. This process was done offline as a preprocessing step before the uncertainty-aware, multi-material, structural topology optimization problem was solved. With the known expressions for the beta random variable statistics, the SROM optimization problem in (19) for uncertainty propagation in forward models is solved to generate $\tilde{\Theta}$ and $\tilde{\Sigma}$ for a range of model sizes $s_\theta = s_\varepsilon = \{5, 10, 15, 20\}$. The CDF and moment error terms, (16) and (18) respectively, are given equal weight in the objective function in (19), i.e. $\alpha_1 = \alpha_2 = 1.0$.

The convergence of the load orientation and elastic modulus SROMs construction problem with increasing SROM size is shown in Figure 2. It is clearly seen that with further refinement of the SROMs, the approximation of the statistics of the underlying random orientation and elastic modulus are improved. Note that the computational cost of the uncertainty aware, multi-material, structural topology optimization problem increases proportionally to the size of the SROMs. Therefore, the smallest SROM representation yielding an acceptable error should be used in practice to minimize the computational cost associated with (21). Figure 2 shows that a relatively small number of samples and probabilities defining $\tilde{\Theta}$ and $\tilde{\Sigma}$ were able to produce a small discrepancy between SROM and target statistics. Indeed, very little improvement in the final objective function value is observed as the SROMs size is increased from 15 to 20. This feature enables the efficient quantification and propagation of the uncertainties introduced by the random inputs during the solution of (21). In Figures 3 and 4, the corresponding load and material SROMs CDFs approximation are compared to the true CDF for different SROM sizes. Clearly, the discrete nature of the SROM

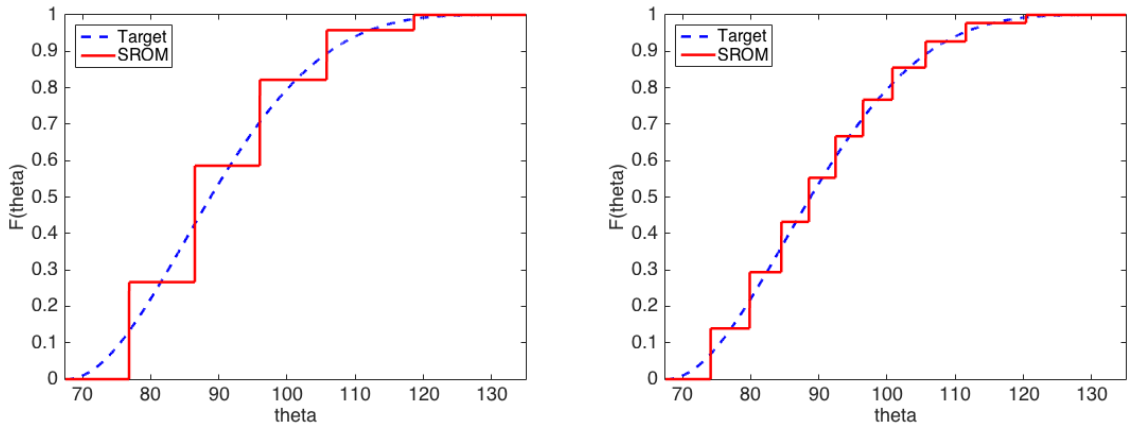

(a) $s_\theta = 5$ (b) $s_\theta = 10$

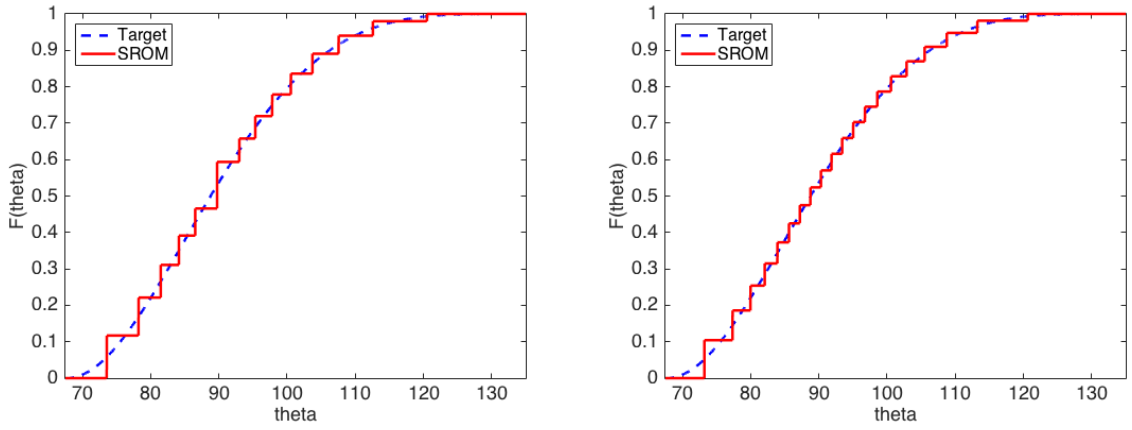

(c) $s_\theta = 15$ (d) $s_\theta = 20$

Figure 3: Comparison of the SROM CDFs with the true distribution of the direction of the applied load, Θ, for different SROM sizes.

approximation improves with increased SROM size.

Finally, the SROM approach was used to design an L-bracket such that the rigidity of the structure was maximized while its mass or cost was minimized. Two candidate materials were used to design the L-bracket. For this design problem, the orientation of the applied load and the elastic modulus of the compliant material were considered to be random. The main design objective is to compute the optimal geometry and placement of the candidate materials such that the design requirements described above are satisfied. Figure 5 compares the optimal geometries obtained by solving (21) with different SROM sizes to the optimal geometries obtained by solving the deterministic multi-material structural topology optimization problem defined in (11). These designs show that the deterministic and uncertainty aware, multi-material, structural topology optimization problems yield different solutions. Indeed, the deterministic solution does not have any additional support material connecting the two main vertical supports (i.e. columns). Contrarily, the uncertainty aware solution places additional support material between the two columns to counter the possibility of a small misalignment in the orientation of the applied load. A small misalignment in the orientation of the applied load could cause unexpected failures due to bending. Furthermore,

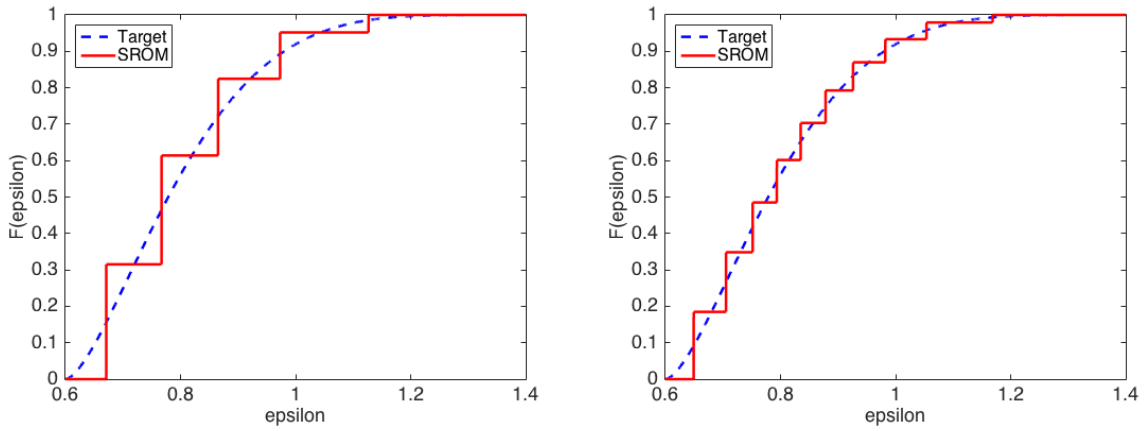

(a) $s_\varepsilon = 5$ (b) $s_\varepsilon = 10$

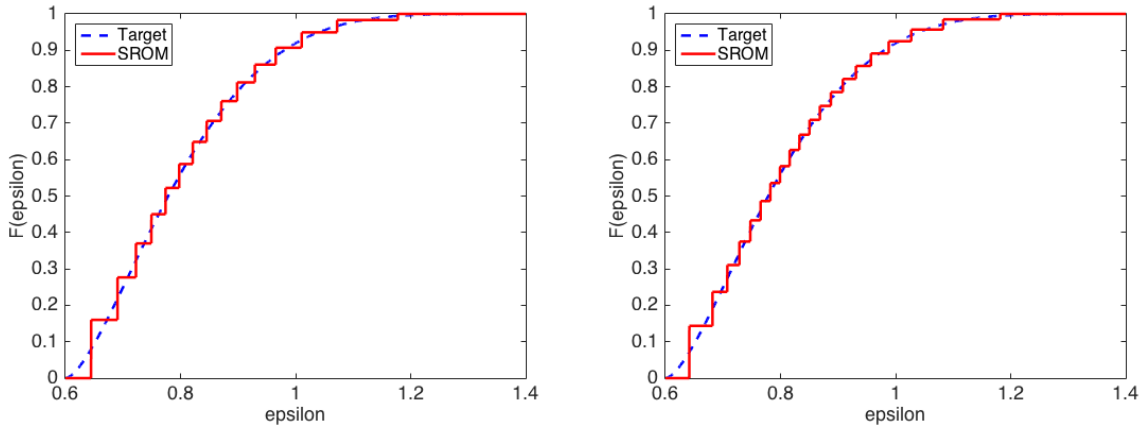

(c) $s_\varepsilon = 15$ (d) $s_\varepsilon = 20$

Figure 4: Comparison of the SROM CDFs with the true distribution of the elastic modulus for the compliant material, Σ, for different SROM sizes.

instead of using the stiff material to produce the additional support structures connecting the two main columns, the algorithm uses mostly soft material to generate the additional support structures. Regardless of the increased deformations due to the randomness in the orientation of the applied load, these deformations are rather small compared to the deformations closer to the applied load. Thus, creating additional support structures made out of soft material is viable since they should be able to withstand the smaller deformations induced by the random orientation in the applied load.

Figure 5 also shows that the support structures made out of soft material are thicker in the deterministic solution than in the uncertainty aware solutions. This is probably induced by the fact that the additional support connecting the two main columns is made out of soft material. Recall that the main design goal is to maximize stiffness such that the mass or cost of the structure is minimize. Therefore, to meet these design requirements, thinner support structures made out of soft material were created. Furthermore, notice that additional stiff support material was added close to the sharp corner in the uncertainty aware solutions shown in Figure 5. This is not only induced by the thinning of the supports made out of soft material, but also by the uncertainty in the elastic modulus of the soft or compliant material. Finally, it is worth pointing out the additional

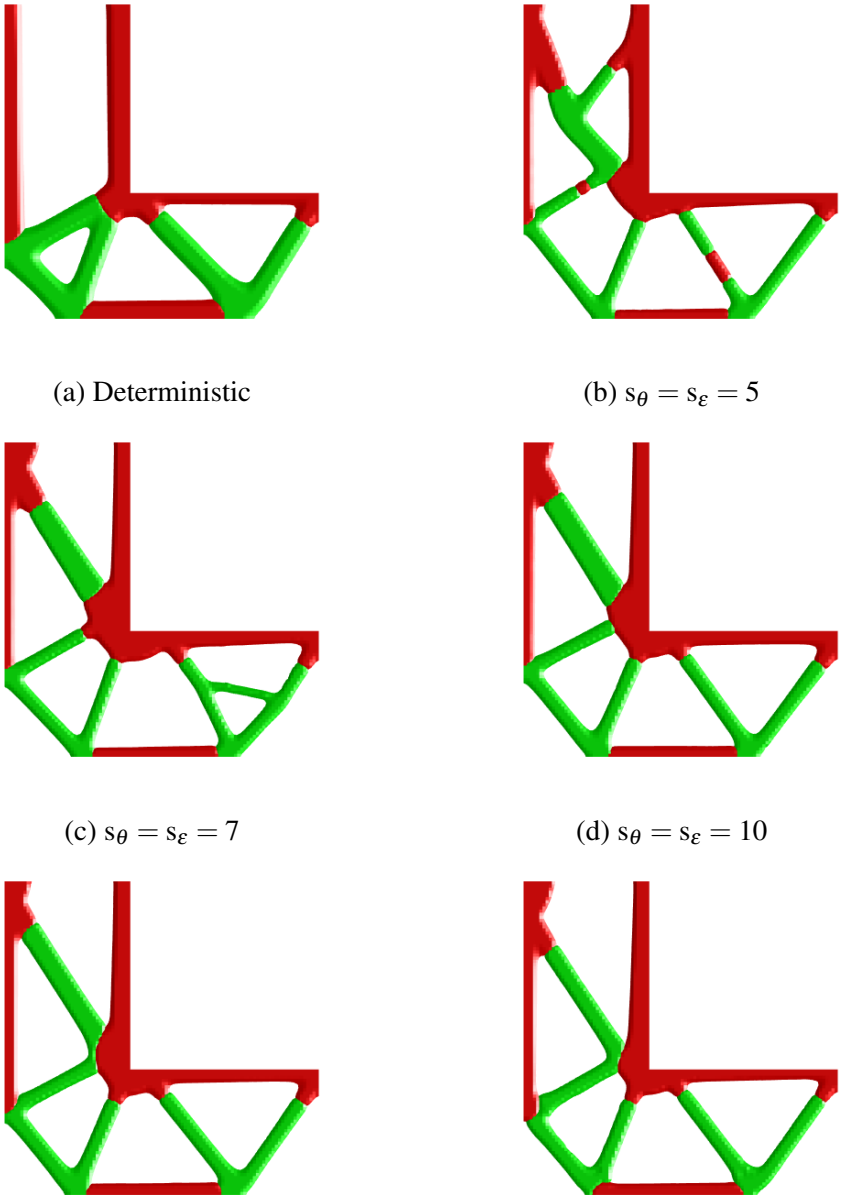

(a) Deterministic

(b) $s_\theta = s_\varepsilon = 5$

(c) $s_\theta = s_\varepsilon = 7$

(d) $s_\theta = s_\varepsilon = 10$

(e) $s_\theta = s_\varepsilon = 15$

(f) $s_\theta = s_\varepsilon = 20$

Figure 5: The optimized topology for increasing SROM sizes for $\tilde{\Theta}$ and $\tilde{\Sigma}$, where red denotes the stiff material and green denotes the soft material. (a) Deterministic solution, where $\tilde{C} \approx 2.808\,e^{-5}$ and Mass ≈ 0.4; (b) Optimized topology for SROMs $\tilde{\Theta}$ and $\tilde{\Sigma}$ of size five, where $\tilde{C} \approx 3.543\,e^{-5}$ and Mass ≈ 0.4; (c) Optimized topology for SROMs $\tilde{\Theta}$ and $\tilde{\Sigma}$ of size seven, where $\tilde{C} \approx 3.757\,e^{-5}$ and Mass ≈ 0.4; (d) Optimized topology for SROMs $\tilde{\Theta}$ and $\tilde{\Sigma}$ of size ten, where $\tilde{C} \approx 3.683\,e^{-5}$ and Mass ≈ 0.4; (e) Optimized topology for SROMs $\tilde{\Theta}$ and $\tilde{\Sigma}$ of size fifteen, where $\tilde{C} \approx 3.632\,e^{-5}$ and Mass ≈ 0.4; and (f) Optimized topology for SROMs $\tilde{\Theta}$ and $\tilde{\Sigma}$ of size twenty, where $\tilde{C} \approx 3.784\,e^{-5}$ and Mass ≈ 0.387.

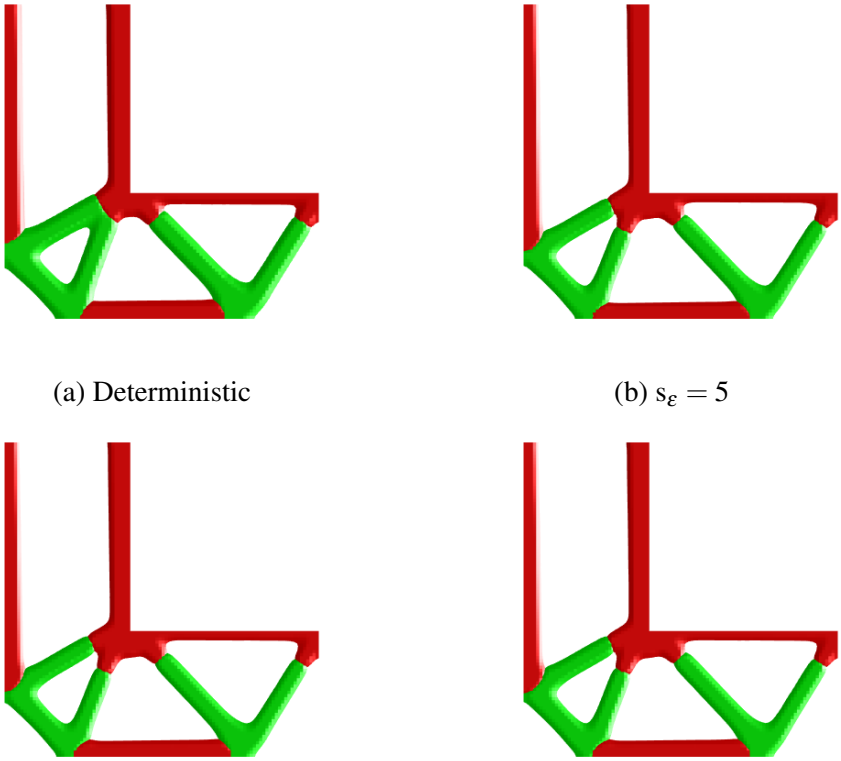

(a) Deterministic (b) $s_\varepsilon = 5$

(c) $s_\varepsilon = 10$ (d) $s_\varepsilon = 15$

Figure 6: The optimized topology for increasing SROM sizes for $\tilde{\Sigma}$, where red denotes the stiff material and green denotes the soft material. (a) Deterministic solution, where $\tilde{C} \approx 2.808\,e^{-5}$ and Mass ≈ 0.4; (b) Optimized topology for SROM $\tilde{\Sigma}$ of size five, where $\tilde{C} \approx 2.828\,e^{-5}$ and Mass ≈ 0.4; (c) Optimized topology for SROM $\tilde{\Sigma}$ of size ten, where $\tilde{C} \approx 2.826\,e^{-5}$ and Mass ≈ 0.4; and (d) Optimized topology for SROM $\tilde{\Sigma}$ of size fifteen, where $\tilde{C} \approx 2.814\,e^{-5}$ and Mass ≈ 0.4.

support added for the case of $s_\theta = s_\varepsilon = 7$ in Figure (c) that isn't present in the other solutions. This is a possible indication that the optimal solution to the stochastic optimization problem is not fully converged with respect to the SROM size until larger values of s_θ and s_ε are used. Indeed, the SROM solutions appear to converge to an optimal geometry in Figures (5.e) and (5.f). In future extensions of the method, a brute force solution will be generated using Monte Carlo simulation and treated as a reference to compare the SROM solutions to and assess convergence in a more rigorous fashion.

Figure 6 shows the optimal geometries obtained by solving an uncertainty aware, multi-material, structural topology optimization problem in the case where only the elastic modulus of the soft material is considered random. The same problem parameters used to solve (21) were used to solve the uncertainty aware, multi-material, structural topology optimization problem with one random parameter. Therefore, the orientation of the applied load was assumed to be known (i.e. deterministic). Similar to the uncertainty aware solutions with two random parameters, the uncertainty aware solutions with one random parameter place more stiff material closer to the sharp corner.

Indeed, the stresses are higher closer to the sharp corner and thus more stiff support material is placed around the sharp corner to insure the design against the random soft material. These examples highlight the importance of accounting for inherent design uncertainties when designing a structure since these uncertainties could cause unexpected failures.

Conclusions

In this study, a novel framework for multi-material structural topology optimization under uncertainty using stochastic reduced order models (SROMs) is proposed. By considering the structural topology optimization problem as a constrained stochastic optimization problem, the approach was formulated in terms of minimizing the expected value of the objective function with a stochastic model constraint. The non-intrusive nature of the SROM approximation transforms the constrained stochastic optimization problem into a deterministic one with decoupled, deterministic physics model constraints. Therefore, the use of SROMs allows for a widely applicable method that relies solely on calls to existing deterministic analysis solvers and optimization libraries. Furthermore, since the model evaluations are completely independent from one another, the approach is embarrassingly parallel and hence scalable to large design problems.

The effectiveness of the proposed SROM framework on a multi-material structural topology optimization problem with a random load and candidate material was demonstrated. Through two numerical examples, the importance of accounting for uncertainties due to multiple inherent design imperfections when designing a structure was shown. Furthermore, the approach can accurately and efficiently quantify and propagate the statistics of a random load and material during optimization. The method was shown to require a small number of samples to characterize the statistics of multiple random inputs, drastically reducing the computational cost associated with the multi-material structural topology optimization problem under uncertainty.

Acknowledgements

Sandia National Laboratories is a multimission laboratory managed and operated by National Technology and Engineering Solutions of Sandia, LLC, a wholly owned subsidiary of Honeywell International, Inc., for the U.S. Department of Energy's National Nuclear Security Administration under contract DE-NA0003525. The information provided in this paper is the sole opinion of the authors and does not necessarily reflect the views of the sponsoring agencies. This document has been reviewed and approved for unclassified, unlimited release under SAND2017-7033C.

References

[1] B. H. Jared, M. A. Aguilo, L. L. Beghini, B. L. Boyce, B. W. Clark, A. Cook, B. J. Kaehr, and J. Robbins, "Additive manufacturing: Toward holistic design," *Scripta Materialia*, vol. 135, pp. 141–147, 2017.

[2] R. G. Ghanem and P. D. Spanos, *Stochastic finite elements: a spectral approach*. Courier Corporation, 2003.

[3] I. Babuška, R. Tempone, and G. E. Zouraris, "Galerkin finite element approximations of stochastic elliptic partial differential equations," *SIAM Journal on Numerical Analysis*, vol. 42, no. 2, pp. 800–825, 2004.

[4] I. Babuška, F. Nobile, and R. Tempone, "A stochastic collocation method for elliptic partial differential equations with random input data," *SIAM Journal on Numerical Analysis*, vol. 45, no. 3, pp. 1005–1034, 2007.

[5] D. M. Frangopol, "Reliability-based optimum structural design," in *Probabilistic structural mechanics handbook*, pp. 352–387, Springer, 1995.

[6] K. Maute and D. M. Frangopol, "Reliability-based design of mems mechanisms by topology optimization," *Computers & Structures*, vol. 81, no. 8, pp. 813–824, 2003.

[7] G. Kharmanda, N. Olhoff, A. Mohamed, and M. Lemaire, "Reliability-based topology optimization," *Structural and Multidisciplinary Optimization*, vol. 26, no. 5, pp. 295–307, 2004.

[8] A. T. Gaynor, N. A. Meisel, C. B. Williams, and J. K. Guest, "Multiple-material topology optimization of compliant mechanisms created via polyjet three-dimensional printing," *Journal of Manufacturing Science and Engineering*, vol. 136, no. 6, p. 061015, 2014.

[9] O. Sigmund and S. Torquato, "Design of materials with extreme thermal expansion using a three-phase topology optimization method," *Journal of the Mechanics and Physics of Solids*, vol. 45, no. 6, pp. 1037–1067, 1997.

[10] O. Sigmund, "Design of multiphysics actuators using topology optimization–Part I: One-material structures," *Computer methods in applied mechanics and engineering*, vol. 190, no. 49, pp. 6577–6604, 2001.

[11] O. Sigmund, "Design of multiphysics actuators using topology optimization–Part II: Two-material structures," *Computer methods in applied mechanics and engineering*, vol. 190, no. 49, pp. 6605–6627, 2001.

[12] "Stratasys." `http://www.stratasys.com`, 2017. Accessed: 2017-06-07.

[13] C. Schumacher, B. Bickel, J. Rys, S. Marschner, C. Daraio, and M. Gross, "Microstructures to control elasticity in 3d printing," *ACM Transactions on Graphics (TOG)*, vol. 34, no. 4, p. 136, 2015.

[14] M. Grigoriu, "Reduced order models for random functions. application to stochastic problems," *Applied Mathematical Modelling*, vol. 33, no. 1, pp. 161–175, 2009.

[15] J. E. Warner, M. Grigoriu, and W. Aquino, "Stochastic reduced order models for random vectors: application to random eigenvalue problems," *Probabilistic Engineering Mechanics*, vol. 31, pp. 1–11, 2013.

[16] M. Grigoriu, "Effective conductivity by stochastic reduced order models (sroms)," *Computational Materials Science*, vol. 50, no. 1, pp. 138–146, 2010.

[17] M. Grigoriu, "Linear random vibration by stochastic reduced-order models," *International journal for numerical methods in engineering*, vol. 82, no. 12, pp. 1537–1559, 2010.

[18] M. Grigoriu, "Solution of linear dynamic systems with uncertain properties by stochastic reduced order models," *Probabilistic Engineering Mechanics*, vol. 34, pp. 168–176, 2013.

[19] J. E. Warner, W. Aquino, and M. Grigoriu, "Stochastic reduced order models for inverse problems under uncertainty," *Computer Methods in Applied Mechanics and Engineering*, vol. 285, pp. 488–514, 2015.

[20] S. Sarkar, J. E. Warner, W. Aquino, and M. D. Grigoriu, "Stochastic reduced order models for uncertainty quantification of intergranular corrosion rates," *Corrosion Science*, vol. 80, pp. 257–268, 2014.

[21] J. M. Emery, R. V. Field, J. W. Foulk, K. N. Karlson, and M. D. Grigoriu, "Predicting laser weld reliability with stochastic reduced-order models," *International Journal for Numerical Methods in Engineering*, vol. 103, no. 12, pp. 914–936, 2015.

[22] E. Lund and J. Stegmann, "On structural optimization of composite shell structures using a discrete constitutive parametrization," *Wind Energy*, vol. 8, no. 1, pp. 109–124, 2005.

[23] J. Stegmann and E. Lund, "Discrete material optimization of general composite shell structures," *International Journal for Numerical Methods in Engineering*, vol. 62, no. 14, pp. 2009–2027, 2005.

[24] T. Gao and W. Zhang, "A mass constraint formulation for structural topology optimization with multiphase materials," *International Journal for Numerical Methods in Engineering*, vol. 88, no. 8, pp. 774–796, 2011.

[25] C. F. Hvejsel and E. Lund, "Material interpolation schemes for unified topology and multi-material optimization," *Structural and Multidisciplinary Optimization*, vol. 43, no. 6, pp. 811–825, 2011.

[26] O. Sigmund and J. Petersson, "Numerical instabilities in topology optimization: A survey on procedures dealing with checkerboards, mesh-dependencies and local minima," *Structural optimization*, vol. 16, no. 1, pp. 68–75, 1998.

[27] O. Sigmund, "Morphology-based black and white filters for topology optimization," *Structural and Multidisciplinary Optimization*, vol. 33, no. 4-5, pp. 401–424, 2007.

[28] T. J. Hughes, *The finite element method: linear static and dynamic finite element analysis*. Courier Corporation, 2012.

[29] M. P. Bendsoe and O. Sigmund, *Topology optimization: theory, methods, and applications*. Springer Science & Business Media, 2013.

[30] M. P. Bendsoe, *Optimization of structural topology, shape, and material*, vol. 414. Springer, 1995.

[31] B. Bourdin, "Filters in topology optimization," *International Journal for Numerical Methods in Engineering*, vol. 50, no. 9, pp. 2143–2158, 2001.

[32] T. E. Bruns and D. A. Tortorelli, "Topology optimization of non-linear elastic structures and compliant mechanisms," *Computer Methods in Applied Mechanics and Engineering*, vol. 190, no. 26, pp. 3443–3459, 2001.

[33] M. Heinkenschloss, "Numerical solution of implicitly constrained optimization problems," TR08-05, Rice University, 6100 Main Street, Houston, TX 77005-1892, 2008.

[34] "The MathWorks Inc. Natick, Massachusetts. MATLAB Version 8.5.0 (R2015a)," 2015.

[35] D. C. Liu and J. Nocedal, "On the limited memory BFGS method for large scale optimization," *Mathematical programming*, vol. 45, no. 1, pp. 503–528, 1989.

[36] Cubit Team, "Cubit, geometry and mesh generation toolkit: version 15.2 user's manual," *Sandia National Laboratories, Tech. Rep. SAND2016-1649 R*, 2016.

[37] M. Heroux, R. Bartlett, V. Howle, R. Hoekstra, J. Hu, T. Kolda, R. Lehoucq, K. Long, R. Pawlowski, E. Phipps, A. Salinger, H. Thornquist, R. Tuminaro, J. Willenbring, and A. Williams, "An Overview of Trilinos," SAND2003-2927, Sandia National Laboratories, P.O. Box 5800, Albuquerque, NM 87185-1110, 2003.

[38] K. Svanberg, "A class of globally convergent optimization methods based on conservative convex separable approximations," *SIAM journal on optimization*, vol. 12, no. 2, pp. 555–573, 2002.